Modelling, Simulation and Validation of thermal propagation for 3D discretized battery cells in Modelica

Finn van Ginneken[1], Alexander Busch[2], Andreas Varchmin[1], Wilhelm Tegethoff[1,2], Juergen Koehler[2]

[1]TLK-Thermo GmbH
Rebenring 31, 38106 Braunschweig
f.van-ginneken@tlk-thermo.com

[2]Institut für Thermodynamik, TU-Braunschweig
Hans-Sommer-Straße 5, 38106 Braunschweig
alexander.busch1@tu-braunschweig.de

Abstract

This publication presents models for dynamic, 3-dimensional simulation of the thermal runaway, thermal propagation and the thermo-electric behavior of battery cells. An optional and replaceable electrical equivalent circuit diagram describes the electrical behavior of the battery cell. Coupled with the 3-dimensional, thermal equivalent circuit diagram, consisting of a resistance-capacitance network, the thermo-electric behavior is represented. A special feature of the battery cell model is the optional, replaceable and physical model of the thermal runaway based on Arrhenius equations and the associated mass loss. This means that either the thermo-electric or the thermal runaway behavior or both can be simulated in combination if required. The anisotropic thermal conductivity of the battery cell and the modelling of relevant heat conduction paths, such as the path across the housing of the battery cell, is made possible by 3D discretization of the battery cell.

Keywords: Lithium-Ion-Battery, thermo-electric Battery model, Arrhenius, Thermal Runway, Dymola, Modelica

1 Introduction

Lithium-ion batteries are used in electrochemical energy storage systems due to properties such as high cycle stability, energy density and capacity at comparatively low costs. However, thermal runaway (TR) can occur in lithium-ion batteries (Lenz et al. 2023; Walker et al. 2022; Groß und Golubkov 2021). This is a chain reaction in which exothermic decomposition reactions lead to exponential self-heating of the battery cell. This fault results in the destruction of the battery cell and, in worst case, can lead to the spread of the fault in the entire system, known as thermal propagation (TP). In addition to the release of heat, there is also a significant release of gas and particles during TR, which leads to a loss of mass in the battery cell. Suitably designed battery systems, particularly their thermal management, can limit the occurrence of faults and thus prevent a TR or at least a TP. The design can be carried out either by means of expensive and time-consuming experiments or by using suitable models (Walker et al. 2022; Groß und Golubkov 2021).

Two modelling approaches for TR are widely used in literature. The first approach is based on empirical heat release models, which can be further subdivided into time-dependent and temperature-dependent models (Hoelle et al. 2023). The advantage of empirical heat releases is the low parameterization and calculation effort (Groß und Golubkov 2021). An overview of other empirical models can be found in Hoelle et al..

The second modelling approach is Arrhenius equation-based models. These models are based on the publication by Hatchard et al. 2001. This model, originally based on two Arrhenius equations, has been extended by various authors for different cell formats and compositions (Kriston et al. 2019; Ren et al. 2018; Wang et al. 2022; MacNeil und Dahn 2001; Lenz 2024). Both modelling approaches (empirical, Arrhenius-based) have advantages and disadvantages. According to Groß und Golubkov the chosen empirical approach has the advantage that no fitting of the Differential Scanning Calorimetry (DSC) curves is necessary and the calculation effort is relatively low even for large battery packs. A decisive disadvantage of empirical modelling is the neglect of the chemical reactions and thus the lack of insight into the reaction cascade. In addition, the TR heat is only released above a certain temperature T_{TR} (Hoelle et al. 2023). As a result, the heat released in the battery cell before the temperature T_{TR} is not considered in the design of thermal management systems.

In addition to the heat release during TR, the modelling of normal operating states is necessary for the design of battery systems and in particular for thermal management (Epp et al. 2022; Epp et al. 2023). Therefore, models for the thermo-electric simulation of pouch and prismatic battery cells are also present. Modelica was chosen as modelling language due to its physical, object-oriented and equation-based characteristics. Several models and libraries are already available for modelling the electrical behavior of a battery cell in Modelica. Einhorn et al. 2013 compared three electrical equivalent circuit models in terms of parameterization effort and accuracy. However, no thermal effects were considered. Gerl et al. 2014 and Uddin und Picarelli 2014 focus on the thermo-electric

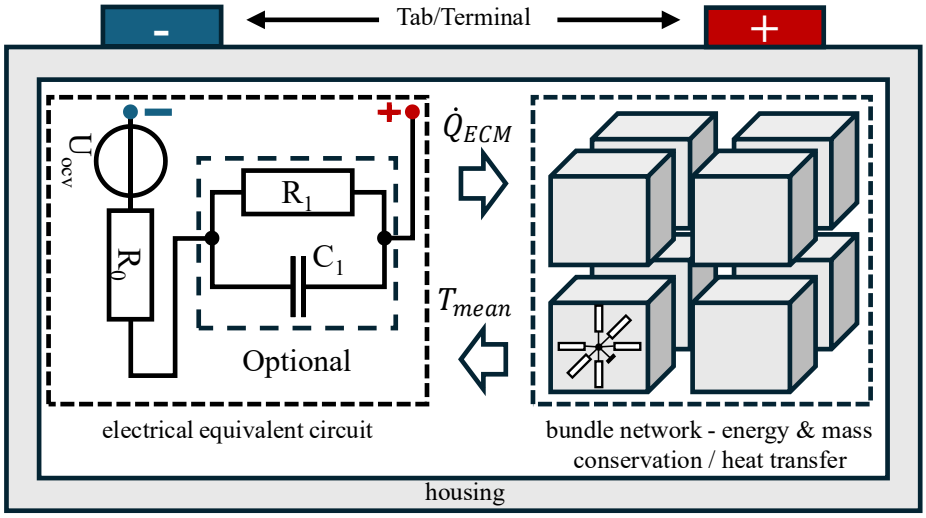

Figure 1. Schematic representation of a prismatic battery cell with the sub models ECM, bundle network, terminal/tab and the coupling of ECM and bundle network

behavior in the respective Modelica library, but do not consider the anisotropic thermal conductivity or the TR. Wendland et al. 2018 address the anisotropic thermal conductivity but does not offer the possibility to consider the TR for individual battery cells. In addition, a point mass can comprise more than one battery cell. The Modelica library by Groß und Golubkov 2021 enables an empirical simulation of the TR, but does not take into account either the anisotropic thermal conductivity or a possible temperature distribution in the battery cell. The library presented by Groß und Golubkov is, to the authors' knowledge, currently the only available library for simulating TR in Modelica.

The models presented in this publication are used for thermo-electric simulation including a TR based on the Arrhenius equation with optional 3D discretization of the battery cell. This allows the anisotropic thermal conductivity and other relevant thermal conduction paths of the battery cell to be considered. In addition, this discretization combines many advantages of high-dimensional flow simulations (CFD) and simplified point mass models.

2 Modelling

The models are combined in the Modelica package named *TIL3_AddOn_Battery*. The package is partly based on the *TIL Suite* and *TILMedia Suite* libraries from TLK-Thermo. In the following, elementary models are presented. Not all models of the package are covered in this publication.

2.1 The Battery Cell

The battery cell model consists of various components (see Figure 1), which are described with sub models. The core of the battery cell is the so-called bundle network, which describes the active material, separators and current collectors in discretized form. No distinction is made between the individual active material layers, separators and current collector foils, so that the bundle network is only parameterized as one material. The bundle network is a replaceable model with 6 heat port matrices consisting of heat ports to enable thermal connection to the housing. The basic 3D control volumes, so-called bundles, are located within the bundle network (see section 2.2). These bundles are instantiated as a 3D matrix. The control volumes are thermally coupled in 3 dimensions in order to address the anisotropic thermal conductivity in the battery cell (Coman et al. 2017; Kim et al. 2021). The discretization is freely selectable.

The bundle network is surrounded by a housing (cf. Figure 1). Apart from the thickness, its discretization is based on the discretization of the bundle network. The housing is not discretized in thickness. A special feature of the housing is the non-structural change of the cell type (pouch-shaped, prismatic). As well as the consideration of the internal heat conduction paths for prismatic housing. For pouch-shaped battery cells, the housing consists of pouch foil. Due to the low foil thickness and to avoid the resulting small-time constants, the foil is modelled as a discretized thermal resistor. For the prismatic battery cell, the heat capacity is considered due to the significantly thicker housing (see Figure 2). By adjusting the internal and external thermal resistance, the heat conduction path can be virtually eliminated depending on the housing. In addition, these resistances are used to model inner/outer foils and to consider reduced thermal conductivity due to the safety valve and/or the terminals for the prismatic battery cell.

The electrical equivalent circuit model (ECM) (see section 2.4 and Figure 1) is globally (not discrete, one ECM per battery cell) integrated in the battery cell and electrically contacted via the two pins. The ECM was not implemented locally due to additional states. For the thermo-electric coupling, the volumetric mean value of the temperatures in the bundle state is used as input. The

DOI 10.3384/ecp218263

heat from the ECM is distributed volumetrically to all bundles. The heat distribution is a simplification; in the event of a thermal runaway, local effects such as short circuits can occur due to a breakdown of the separator (Kim et al. 2021); these effects cannot be modelled by the ECM.

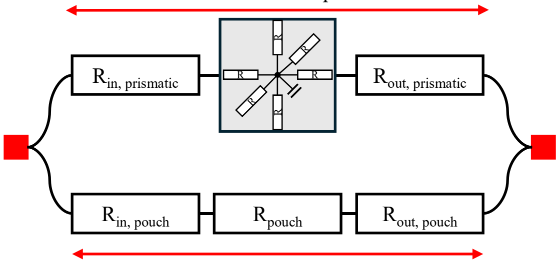

Figure 2. Representation of the heat conduction paths for housing of a prismatic or pouch battery cell

In addition, the battery cell model also contains connectors for electrical and thermal contact to the outside and one model each for the positive and negative tab or terminal (not described in the following).

2.2 The Li-Ion-Bundle

The Li-Ion-Bundle is the basic model for the bundle network. This bundle is based on the thermal bundle and the same assumptions apply; constant geometric volume. It also has 6 heat ports, 6 thermal resistors and a thermal capacitance. The thermal bundle is the basis for many other components (such as housing or layers).

The heat flows via the heat ports are described by the following equation.

$$\dot{Q}_i = 2\left(\frac{T_{port,i} - T}{R_{th,i}}\right) \tag{1}$$

$T_{port,i}$ represents the temperature at the respective heat port, T the temperature state of the bundle. $R_{th,i}$ describes the thermal resistance between the temperature state and the heat port depending on thermal conductivity (in the respective spatial direction), distance and relevant cross-sectional area.

Furthermore, each bundle has a solid model for calculation of properties. The solid itself is replaceable and both temperature-dependent and constant properties can be specified for the thermal conductivity and specific heat capacity. For the temperature-dependent specific heat capacity c_p, specific solid enthalpy h_s must be determined as follows:

$$h_s = c_{p,nom}T_{nom} + \int_{T_{nom}}^{T} c_{p,s}\,dT \tag{2}$$

T_{nom} is the nominal temperature and $c_{p,nom}$ is the nominal specific heat capacity of the solid. Integration via the temperature is done in Modelica using the trapezoidal or Simpson's rule, which is implemented in a function.

The main differences between the thermal and Li-Ion-bundles are the TR model and the variable solid volume within the Li-Ion-bundle. In the optional, replaceable TR model, a mass-specific heat flow $\dot{q}_{TR}$ and a change of the relative degree of conversion $\dot{\gamma}_{rel,out}$ are calculated (see section 2.3). These variables are decisive for the mass and energy balance. The mass balance for a Li-Ion-bundle is given by the following equation.

$$\frac{dm_s}{dt} = V_s\frac{d\rho_s}{dt} + \rho_s\frac{dV_s}{dt} = m_{s,initial}\dot{\gamma}_{rel,out} \tag{3}$$

m_s represents the solid mass of the bundle. For normal operation, the mass of the solid is constant ($dm_s/dt = 0$). In the case of TR, the Li-Ion-bundle can eject mass in form of gases, electrolyte droplets and particles. Consequently, $dm_s/dt \neq 0$ applies. The dynamic mass loss is described by the change of the relative degree of conversion $\dot{\gamma}_{rel,out}$ (cf. equation 12), multiplied by the initial solid mass $m_{s,initial}$. The ejected mass does not differentiate between gases, electrolyte droplets or particles. So that there is only one outgoing mass flow. This mass flow is not considered further at present.

Another assumption is that the solid density ρ_s is constant. However, to address the ejected mass, the volume of the solid V_s must be variable. Since the active material is a porous structure (Kim et al. 2021) and in order to avoid having to normalize the solid volume, the porosity ϕ is chosen as the differential state. The porosity is typically 10 % - 30 % (Kim et al. 2021) and represents the ratio of void volume V_H to geometric volume V. It is defined as follows:

$$\phi = \frac{V_H}{V} = \frac{V - V_s}{V} \qquad V_s = V(1-\phi) \tag{4}$$

By taking these assumptions and substituting the solid volume, the mass balance for the Li-Ion-bundle follows (see equation 5). The differential state for porosity can be avoided by suitable transformations (see section 2.3). It is assumed that the porosity has no influence on thermal conductivity or specific heat capacity. The authors are not aware of any publications in which changes in thermal conductivity due to changes in porosity during TR in the battery cell have been investigated.

$$\rho_s V\frac{d\phi}{dt} = -m_{s,initial}\dot{\gamma}_{rel,out} \tag{5}$$

In addition to the mass balance, the energy balance is decisive (see equation 6). This is determined by the enthalpy flow due to the ejected mass, the TR heat $\dot{q}_{TR}$

(see section 2.3), the ECM heat $\dot{Q}_{ECM}$ (see section 2.4) and the heat across the balance boundaries. For the enthalpy flow, it is assumed that the ejected mass carries the same specific enthalpy as the solid has at the time ($h_{s,out} = h_s$).

$$\begin{aligned}\frac{dU_s}{dt} = &\sum_{i=1}^{6} \dot{Q}_i + \dot{Q}_{ECM} \\ &+ m_s \dot{q}_{TR} + m_{s,initial} \dot{Y}_{rel,out} h_{s,out} \\ &- p \frac{dV_s}{dt}\end{aligned} \tag{6}$$

Equation 6 represents the energy balance according to the first law of thermodynamics, neglecting potential and kinetic energy. The relationship between the solid enthalpy H_s and the internal energy $U_s = H_s - pV_s$ leads to the following total differential.

$$\frac{dU_s}{dt} = \frac{dH_s}{dt} - p\frac{dV_s}{dt} - V_s\frac{dp}{dt} \tag{7}$$

Where p describes the pressure. Due to the pressure-independent properties of the solid, only $dU_s = dH_s - pdV_s$ remains. By inserting the relationship (cf. equation 7) into equation 6, the work of volume change pdV_s is reduced and the following total differential of the solid enthalpy remains on the left-hand side.

$$\frac{dH_s}{dt} = m_s\frac{dh_s}{dt} + h_s\frac{dm_s}{dt} \tag{8}$$

With the mass balance and the assumption for the enthalpy flow carried along, equation 6 can be simplified to the following implemented equation.

$$m_s\frac{dh_s}{dt} = \sum_{i=1}^{6} \dot{Q}_i + \dot{Q}_{ECM} + m_s\dot{q}_{TR} \tag{9}$$

2.3 The Thermal Runaway Model

Another central element of the battery cell is the calculation of the TR. For this purpose, a base class has been implemented to enable the replacement of different TR models. This means that new TR models can be easily integrated. The base class implementation targets Arrhenius equation based TR models, but can be easily adapted to empirical models, such as the one by Groß und Golubkov.

One of the most important inputs in the TR model is temperature. The decisive output is the mass-specific heat flow. This is determined by the change in the degree of conversion of the reactions. In literature, the degree of conversion is often referred to as dimensionless concentrations. The output and the implementation are illustrated below using the publication by Ren et al..

In the mentioned publication, DSC measurements are carried out for various battery cell components (cathode, anode, electrolyte). Using these measurements at different heating rates and the Kissinger or Flynn-Wall-Ozawa method, the kinetic triplet for specific DSC-peaks is derived (Ren et al. 2018). The decisive kinetic triplet (equation 10) consists of frequency parameter A_x, activation energy $E_{A,x}$ and reaction model f.

$$\begin{aligned}\kappa_x &= A_x \exp\left(-\frac{E_{A,x}}{RT(t)}\right) \\ \frac{d\alpha_x}{dt} &= -\kappa_x f \\ f &= \alpha_x^{n_x} \\ &\quad \cdot (1-\alpha_x)^{m_x} \\ &\quad \cdot (-\ln(1-\alpha_x))^{p_x} \\ \alpha_x(t=0) &= 1, \qquad \alpha_x \in [0,1]\end{aligned} \tag{10}$$

κ_x represents the respective conversion rate described by the Arrhenius equation. α_x is the degree of conversion of the approximated x-th DSC peak. f represents the kinetics-dependent reaction model, which describes the thermal decomposition of the solid. The exponents are used to represent different reaction models, such as the autocatalytic reaction ($n_x = 1, m_x = 1$) (Al-Khamis et al. 2010; MacNeil und Dahn 2001).

For the TR model of Ren et al., a power law reaction model with variable reaction order n_x is assumed for the reaction model ($p_x = 0, m_x = 0$). Six dominant DSC peaks are found in the publication and an ordinary differential equation (ODE) is implemented accordingly. The correct implementation can be verified by specifying a heating rate (via the temperature input) and then comparing the modelled with the measured DSC peak. The superposition of the modelled DSC peaks enables the determination of the resulting, mass-specific total heat flow $\dot{q}_{TR}$ (see equation 11). Figure 3 shows the simulated mass-specific total heat flow of the using equation 11 (for the DSC-simulation the reactive mass is set to one) compared to the DSC-measurement of the anode-electrolyte sample by Ren et al.

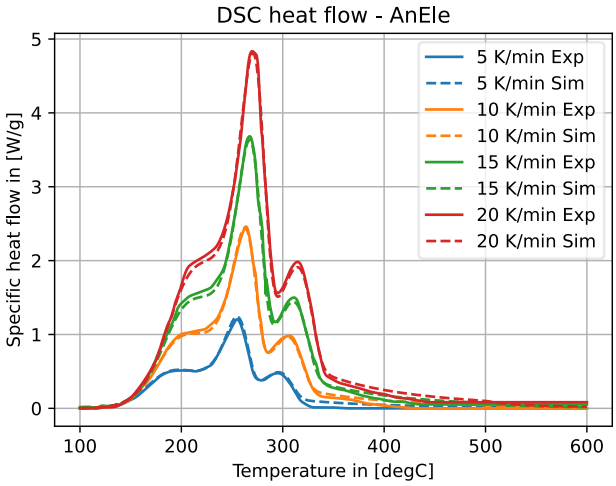

Figure 3. Comparison between modelled and measured specific heat flows for different heating rates

DOI 10.3384/ecp218263

The reaction enthalpy $\Delta h_{R,x}$ in equation 11 is the integral under the specific DSC-peak and n describes the number of peaks considered. $\varphi_{reactive}$ describes the reactive mass in the battery cell and is 55.3 % according to Ren et al..

$$\dot{q}_{TR} = \varphi_{reactive} \sum_{x=1}^{n} \Delta h_{R,x} \frac{d\alpha_x}{dt} \tag{11}$$

The relative change $\dot{\gamma}_{rel,out}$ must be defined for the ejected mass (see section 2.2). Therefore, the change of a specific degree of conversion or an average value from several degree of conversions can be used. A relative, dynamic mass loss is thus determined using the equation 12. φ_{loss} represents the relative mass loss of the battery cell.

$$\dot{\gamma}_{rel,out} = \frac{\varphi_{loss}}{n} \sum_{x=1}^{n} \frac{d\alpha_x}{dt} \tag{12}$$

By inserting the conversion degrees into equation 12, not the derivative, the already relative, ejected mass is described, so that equation 5 can be simplified to the following equation. This avoids the porosity state for each Li-Ion-bundle.

$$\rho_s V \phi = m_{s,initial} \cdot \left(1 - \frac{\varphi_{loss}}{n} \sum_{x=1}^{n} \alpha_x\right) \tag{13}$$

From a numerical perspective, it is useful to limit the conversion rate κ_x. The influence on the heat release should be as low as possible. The limitation via a time constant is not expedient in this case, as this is dependent on the temperature (see equation 14). For this reason, the numerical limitation is carried out using the characteristic time τ. For equation 14 a linear DGL was assumed for simplifications. The characteristic time is limited to $\tau_{min} = 10\,ms$. This time has proven to be a good compromise between numerical solvability and influence on the heat release.

$$\begin{gathered} \frac{d\alpha_x}{dt} = -\kappa_x \alpha_x \\ a_x = a_{x,t=0} e^{-\frac{t}{\tau}} = a_{x,t=0} e^{-\kappa_x t} \\ \tau = \frac{1}{\kappa_x} \\ \frac{d\alpha_x}{dt} = \begin{cases} -\kappa_x \alpha_x, & \kappa_x < \frac{1}{\tau_{min}} \\ -\frac{1}{\tau_{min}} \alpha_x, & \kappa_x \geq \frac{1}{\tau_{min}} \end{cases} \end{gathered} \tag{14}$$

2.4 The Electrical Equivalent Circuit Model

A replaceable ECM was chosen for the battery cell. The reasons for choosing an ECM are accurate description of the electrical behaviour and the released heat with low computational effort (Auch et al. 2023; Einhorn et al. 2013) as well as the direct possibility of parameter identification in Modelica (Einhorn et al. 2013; Uddin und Picarelli 2014). The currently implemented ECM are based on the publications by Einhorn et al. and Gerl et al.. They include the Rint (Ri), Thevenin (Th) and Dual Polarization Model (DP) (cf. Figure 4). These models have advantages and disadvantages depending on the accuracy and performance requirements (Einhorn et al. 2013). All ECM's use the same base class, which consists of several components such as a voltage source, resistors and current interrupt devices (CID). The CID decouples the ECM from the electrical pins at high temperatures, e.g. triggered by the TR. The voltage source U_{OCV} describes the open circuit voltage (OCV). The resistors describe several effects. R_0 represents the ohmic internal resistance of the battery cell. The terminal voltage U_T must be calculated differently depending on the model selected (see Figure 4).

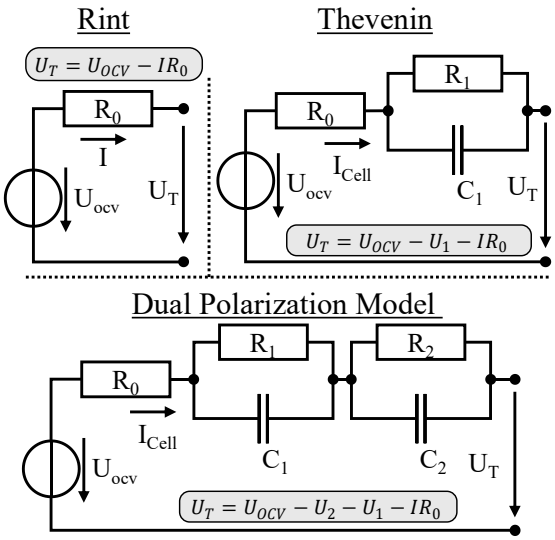

Figure 4. Schematic representation of the ECMs

The electrical data for the OCV, resistances and capacitances can be constant, equation-based or table-based. Whereby the look-up table enables 2D interpolation to consider the SoC and temperature dependence of the data (cf. Einhorn et al. 2013; Uddin und Picarelli 2014). The SoC is determined by Coulomb counting. According to Bernardi et al. 1985 the released heat is described by the irreversible $\dot{Q}_{Loss}$ and reversible $\dot{Q}_{Rev}$ heat. The irreversible part includes ohmic losses, charge transfer, overpotentials and the limitation of mass transfer. The reversible part includes entropy changes and is described by the partial derivative of the OCV with respect to temperature $\frac{\partial U_{OCV}}{\partial T}$ (ϵ small temperature delta) (Auch et al. 2023; Bernardi et al. 1985).

$$\begin{aligned} \dot{Q}_{ECM} &= \dot{Q}_{Loss} + \dot{Q}_{Rev} \\ \dot{Q}_{Loss} &= \mathrm{I}(\mathrm{U_{OCV}} - U_T) \\ \dot{Q}_{Rev} &= IT\frac{\partial \mathrm{U_{OCV}}}{\partial \mathrm{T}} \\ \frac{\partial \mathrm{U_{OCV}}}{\partial \mathrm{T}} &= \frac{\mathrm{U_{OCV}}(T+\epsilon) - \mathrm{U_{OCV}}(T-\epsilon)}{2\epsilon} \end{aligned} \tag{15}$$

2.5 States and Sparse Solvers

The number of differential states changes depending on the discretization. For each thermal and Li-Ion-bundle there is exactly one differential state, the temperature. The porosity can be replaced by an algebraic expression (see section 2.3). Thus, the number of states for the bundle network and housing depends on the discretization. In addition, there is one state each for the tabs/terminals. The Dymola sparse solver (Dassault Systèmes AB 2025) can help speed up the simulation. For example, a TR simulation of a 125-fold discretized battery cell without sparse solver takes ~36 s, with only ~15 s (on a laptop with an 11th Gen Intel Core i7-11800H - 2.30GHz and 16 GB RAM). Thus, the simulation time for this case can be reduced by approx. 42 % by using a sparse solver. A 1000-fold discretization of a battery cell is possible, but the simulation time increases to 2700 s and the DAE system 133408 scalar equations. Higher discretization's were not tested. A comparison with an CFD simulation has not yet been conducted.

By using a global TR model (not discretized one per battery cell) the number of states can be greatly reduced, which can be helpful when simulating entire battery systems. The model shows that Modelica and Modelica tools should continue to improve dealing with high discretization, since the translation time increases exponentially with the number of states, even though the bundles all consist of the same code. This challenge has been recognized and is being addressed in the European OpenSCALING 2023 project.

3 Experiment

The battery cell model described in Section 2.1 can be used to model normal operating behavior with charging and discharging processes as well as dynamic load profiles (Epp et al. 2022; Epp et al. 2023). In addition to simulating the normal operating behavior, it is also possible to carry out safety analyses for the event of damage to TP. These safety considerations can be used for the development of thermally safer battery systems. Furthermore, applications in model-based early detection of the TP are conceivable.

In this section, the *TIL3_AddOn_Battery* is checked for plausibility by comparing it with an experimental propagation test. The test by Schöberl et al. 2024 is used for comparison. This plausibility check concentrates on the thermal propagation. A simulation of the electrical behavior coupled with the thermal behavior is not carried out.

3.1 Propagation Experiment Setup

In the experimental propagation test by Schöberl et al. two battery cell types are examined with regard to their thermal propagation behavior. The battery cells investigated are nickel-manganese-cobalt (NMC)-811 and lithium iron phosphate (LFP). The measurement results for NMC-811 are considered below.

In the experiment, five cells were mounted between two steel plates with two additional thermal insulation layers. The cells are not electrically connected to each other. The battery cells were tensioned with a SoC of 30 %. The battery cells are wrapped in a thin insulating film. Vermiculite plates were used as thermal insulation layers. A heater was placed between one of the insulating layers and the neighboring battery cell to trigger the TR in the first cell. The TR in the first battery cell provided enough heat to trigger the TR in the other cells. By measuring the temperature between the cells, between the first cells it was possible to trace the propagation process

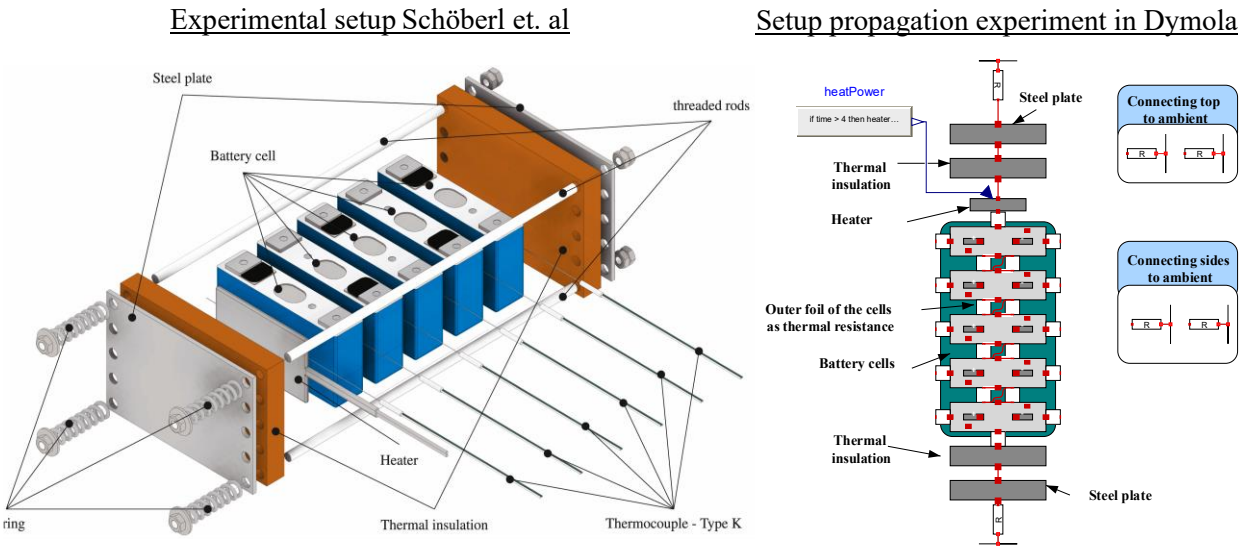

Figure 5. Propagation experiment by Schöberl et al. and the transfer of the setup to Modelica diagram

DOI 10.3384/ecp218263

in the experiment. The structure described is shown in Figure 5.

The steel plates, the thermal insulation layers and the heater are modelled as layers using the thermal bundles (see section 2.2). With the help of the *TILMedia Suite*, a material can be assigned to the layers via the replaceable *SolidType* record. As in the experiment, the dimensions of the layers are adapted to the cell size with an additional allowance, which is estimated using the illustrations from Schöberl et al.. In addition to the thermal insulation layers visible in Figure 5, a further insulation layer is placed on the undersides of the cells. The power for the heater is provided via input. The specified heat flow per area is selected as in the publication. Schöberl et al. specifies that the heater is switched off manually if the TR has occurred in the first cell. In the simulation setup, the heater is switched off at a defined temperature T_{off}.

The model described in section 2.1 is used for battery cells. The foils with which the battery cells are wrapped are modelled in the simulation experiment using thermal resistors.

The TR model (see section 2.3) of the battery cell used for the simulation is parameterized using Ren et al.. The parameters specified in the publication were determined for cell chemistry of NMC-111 and a different battery cell type. The model therefore needs to be adapted. The relative mass loss φ_{loss} and the factor for the relative mass of the cell that can decompose in the TR reaction $\varphi_{reactive}$ are adjusted. The estimation of the reactive mass $\varphi_{reactive}$ was based on the temperature levels available from the measurements. The mass loss is described in Schöberl et al. for all five cells with an average of $\varphi_{loss} =$ 45,8 %. For the individual cells, the relative mass loss is stored in the TR model.

The heat ports of the battery cells and the heater, which are not visibly connected to another heat port in Figure 5 are connected to the environment via a convection resistor. Table 1 shows the details of the individual models with their respective properties for the simulation.

Table 1. Summary of the relevant values for the propagation simulation

Symbol	Description	Value	Literature
General			
T_{Start}	Initialization & ambient temperature	20 °C	Assumption
T_{off}	Heater switch-off temperature	375 °C	Assumption
$\dot{q}_{HT}$	Heat output per heating surface	6.2 $\frac{W}{cm^2}$	Schöberl et al. 2024
α_{Air}	Heat transfer coefficient for convection resistance	12 $\frac{W}{m^2K}$	Assumption
Steel Plate (TILMedia-Stainless Steel)			
$n_{x,St}$,$n_{y,St}$,$n_{z,St}$	Discretization in x-, y- and z-direction	1, 1, 1	-
δ_{St}	Thickness	5 mm	Assumption
$c_{p,St}$	Specific heat capacity	450 $\frac{J}{kgK}$	TIL-Media
λ_{St}	Thermal conductivity	14.6 $\frac{W}{mK}$	TIL-Media
ρ_{St}	Density	7900 $\frac{kg}{m^3}$	TIL-Media
Thermal insulation layer (Vermiculite)			
$n_{x,TI}$,$n_{y,TI}$,$n_{z,TI}$	Discretization in x-, y- and z-direction	1,1,1	-
δ_{TI}	Thickness	25 mm	Schöberl et al. 2024
$c_{p,TI}$	Specific heat capacity	960 $\frac{J}{kgK}$	*Datasheet
λ_{TI}	Thermal conductivity	0.071 $\frac{W}{mK}$	*Datasheet
ρ_{TI}	Density	176 $\frac{kg}{m^3}$	*Datasheet
Heater (TILMedia-Aluminium)			
$n_{x,Ht}$,$n_{y,Ht}$,$n_{z,Ht}$	Discretization in x-, y- and z-direction	1,1,1	-
δ_{Ht}	Thickness	0.5 mm	Assumption
$c_{p,Ht}$	Specific heat capacity	920 $\frac{J}{kgK}$	TILMedia
λ_{Ht}	Thermal conductivity	215 $\frac{W}{mK}$	TILMedia
ρ_{Ht}	Density	2700 $\frac{kg}{m^3}$	TILMedia
Battery Cell NMC-811 / 173 x 42 x 85 mm (Housing material: TILMedia-Aluminium)			
$n_{x,Bz}$,$n_{y,Bz}$,$n_{z,Bz}$	Discretization in x-, y- and z-direction	3,15,1	-
m_{Bz}	Average mass	1423.9 g	Schöberl et al. 2024
$c_{p,Bz}$	Specific heat capacity	800 $\frac{J}{kgK}$	Assumption
$\lambda_{Bz,\parallel}$	Thermal conductivity parallel to the active material layers	23.1 $\frac{W}{mK}$	Hoelle et al. 2023
$\lambda_{Bz,\perp}$	Thermal conductivity across the active material layers	1.034 $\frac{W}{mK}$	Hoelle et al. 2023
$\lambda_{Bz,Foil}$	Thermal conductivity of outer foil	0.25 $\frac{W}{mK}$	Assumption
$\delta_{Bz,Foil}$	Thickness outer foil	0.05 mm	Assumption
$\varphi_{reactive}$	Reactive mass TR model	38 %	Assumption
φ_{loss}	Average mass loss	45.8 %	Schöberl et al. 2024

*Datasheet: Vermiculite Association

3.2 Simulation Results

For the plausibility check of the models, the temperatures between the battery cells are examined as in the experiment. The temperatures at the respective heat ports of the cell models can be used for this purpose. The simulation results compared to the measurement data are shown in Figure 6. In the simulation, all five cells enter the TR, and a TP could be shown.

The simulation and the experiment show a good agreement for the initial temperature rise of the TR for the first three battery cells. This shows that heat conduction is well represented for the first three battery cells and that TR heat is released at a temperature comparable to the experiment. However, some deviating temperature curves are recognizable. A comparison between T1 measurements and T1 simulation shows a slower heating phase for the simulation. The reasons for this may lie in the lack of information on the internal cell structure or in

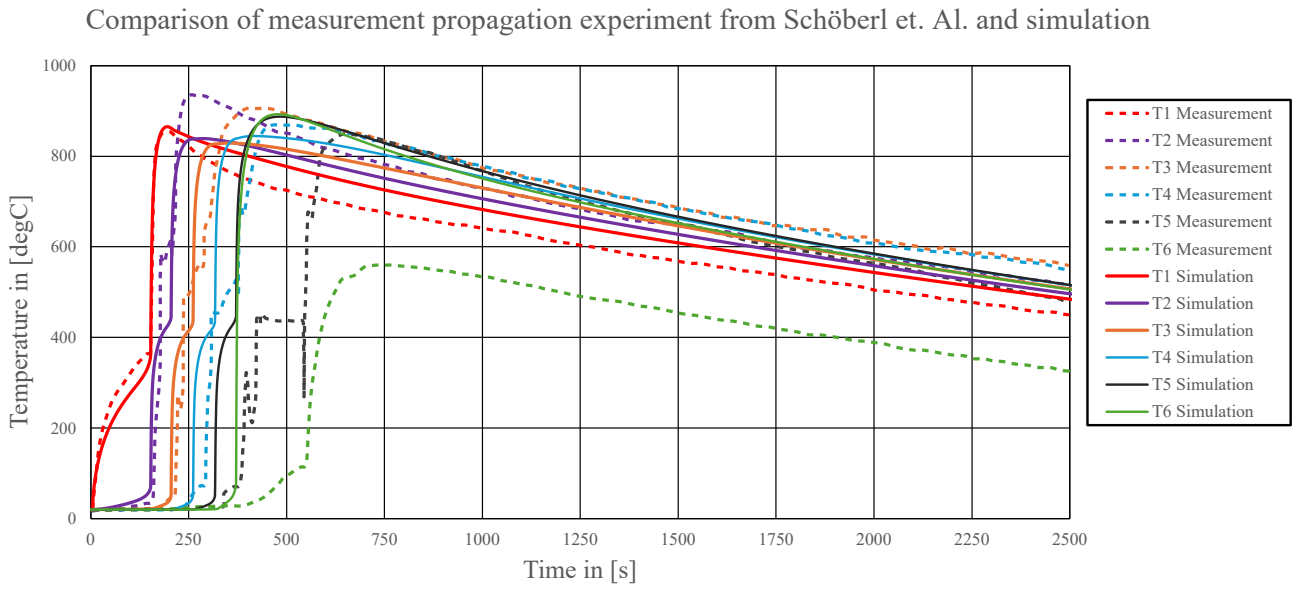

Figure 6. Comparison measurement (Schöberl et al. 2024) and simulation (T1-Heater-Cell 1; T2- Cell 1-Cell 2; T3- Cell 2-Cell 3; T4- Cell 3-Cell 4; T5- Cell 4-Cell 5; T6- Cell 5-Insulation)

deviating thermal properties due to assumptions made during modelling. Furthermore, the temperature for the measurement after the TR in cell 1 drops faster than in the simulation. In Schöberl et al. the mass loss could only be estimated retrospectively for the first cells. The mass loss of the first three cells was averaged due to irreversible fusion. If cell 1 has emitted more mass in the experiment than assumed, this can lead to the recognizable deviating cooling behavior. In the cooling phase of the other cells after the TP, similar temperature curves are observed between simulation and measurement.

The behavior of cell 5 cannot be matched with the simulation. The temperature rise in the TR stagnates here. One reason could be the decomposition reactions which are subject to a certain scatter (Lenz et al. 2023). Another reason could be the loss of mechanical integrity due to the mass loss and a resulting thermal contact resistance between the battery cells where the temperature is measured (Schöberl et al. 2024). This could also be the reason for the different temperature curve between simulation and measurement in cell 6. In addition, the temperature of cell 6 is significantly influenced by cell 5.

The simulation is based on several assumptions (cf. Table 1). The mentioned deviations in temperature curves can arise due to deviating thermal properties of the assumed material parameters. To make the simulation more reliable, the materials used should be thermally characterized in advance for a battery system to be investigated. In conclusion, it can be said that a TP can be simulated with the battery library and that these simulations can be used to carry out safety assessments for battery systems.

4 Conclusion

This publication presents a discretized 3D battery cell model in Modelica. The focus of the modelling is the physical simulation of the TR based on the Arrhenius equations and the modelling of the anisotropic thermal conductivity. This allows to consider relevant heat conduction paths in the battery cell using 3D discretization. The thermo-electric behavior is modelled by a coupled ECM. The model was developed for the user-friendly and fast simulation of battery cells and systems. To the authors' knowledge, the 3-dimensional thermal calculation with a coupled physical TR model is a novel approach in Modelica for the simulation of battery systems. The comparison with an experiment from the literature has shown good agreement with the simulation. The calculation of the TP was possible within approx. 83 s (experimental time approx. 47 min) and thus represents only a fraction of the required simulation time compared to complex 3D CFD simulations.

Future enhancements of battery cell model are gas generation, outgassing and particle ejection, which have a significant influence on the TR. As well as further components and exemplary models for simulation of entire battery systems.

Acknowledgements

This work has been supported by German Federal Ministry of Education and Research (BMBF, Grant No.: 01IS24045A).

References

Al-Khamis, Kh.M.; Al-Othman, Z. A.; Mahfouz, R. M. (2010): Kinetic Studies of the Non-Isothermal Decomposition of Unirradiated and Γ-Irradiated Gallium Acetylacetonate. In: *Progress in Reaction Kinetics and Mechanism* 35 (2), S. 187–207. DOI: 10.3184/146867810X12686717520239.

Auch, Marcus; Kuthada, Timo; Giese, Sascha; Wagner, Andreas (2023): Influence of Lithium-Ion-Battery Equivalent Circuit Model Parameter Dependencies and Architectures on the Predicted Heat Generation in Real-Life Drive Cycles. In: *Batteries* 9 (5), S. 274. DOI: 10.3390/batteries9050274.

Bernardi, D.; Pawlikowski, E.; Newman, J. (1985): A General Energy Balance for Battery Systems. In: *J. Electrochem. Soc.* 132 (1), S. 5–12. DOI: 10.1149/1.2113792.

Coman, Paul T.; Darcy, Eric C.; Veje, Christian T.; White, Ralph E. (2017): Modelling Li-Ion Cell Thermal Runaway Triggered by an Internal Short Circuit Device Using an Efficiency Factor and Arrhenius Formulations. In: *J. Electrochem. Soc.* 164 (4), A587-A593. DOI: 10.1149/2.0341704jes.

Dassault Systèmes AB (Hg.) (2025): Dymola - Full User Manual (2025x). All Chapters from User Manual 1A – User Manual 2C Included). Ideon Gateway, Scheelevägen 27 – Floor 9, SE-223 63 Lund, Sweden.

Einhorn, Markus; Conte, Fiorentino Valerio; Kral, Christian; Fleig, Jürgen (2013): Comparison, Selection, and Parameterization of Electrical Battery Models for Automotive Applications. In: *IEEE Trans. Power Electron.* 28 (3), S. 1429–1437. DOI: 10.1109/TPEL.2012.2210564.

Epp, Alexander; Rai, Sunny; van Ginneken, Finn; Varchmin, Andreas; Koehler, Juergen; Sauer, Dirk Uwe (2023): Simulative Investigation of Optimal Multiparameterized Cooling Plate Topologies for Different Battery System Configurations. In: *Energy Tech* 11 (9), Artikel 2300405. DOI: 10.1002/ente.202300405.

Epp, Alexander; Wendland, Robert; Behrendt, Jan; Gerlach, Robin; Sauer, Dirk Uwe (2022): Holistic battery system design optimization for electric vehicles using a multiphysically coupled lithium-ion battery design tool. In: *Journal of Energy Storage* 52, S. 104854. DOI: 10.1016/j.est.2022.104854.

Gerl, Johannes; Janczyk, Leonard; Krüger, Imke; Modrow, Nils (2014): A Modelica Based Lithium Ion Battery Model. In: Proceedings of the 10th International Modelica Conference, March 10-12, 2014, Lund, Sweden. the 10th International Modelica Conference, March 10-12, 2014, Lund, Sweden, March 10-12, 2014: Linköping University Electronic Press (Linköping Electronic Conference Proceedings), S. 335–341.

Groß, Christian; Golubkov, Andrej W. (2021): A Modelica library for Thermal-Runaway Propagation in Lithium-Ion Batteries. In: Proceedings of 14th Modelica Conference 2021, Linköping, Sweden, September 20-24, 2021. 14th Modelica Conference 2021, 2021-09-20: Linköping University Electronic Press (Linköping Electronic Conference Proceedings), S. 215–224.

Hatchard, T. D.; MacNeil, D. D.; Basu, A.; Dahn, J. R. (2001): Thermal Model of Cylindrical and Prismatic Lithium-Ion Cells. In: *J. Electrochem. Soc.* 148 (7), A755. DOI: 10.1149/1.1377592.

Hoelle, S.; Zimmermann, S.; Hinrichsen, O. (2023): 3D Thermal Simulation of Thermal Runaway Propagation in Lithium-Ion Battery Cell Stack: Review and Comparison of Modeling Approaches. In: *J. Electrochem. Soc.* 170 (6), S. 60516. DOI: 10.1149/1945-7111/acd966.

Kim, Jinyong; Mallarapu, Anudeep; Finegan, Donal P.; Santhanagopalan, Shriram (2021): Modeling cell venting and gas-phase reactions in 18650 lithium ion batteries during thermal runaway. In: *Journal of Power Sources* 489, S. 229496. DOI: 10.1016/j.jpowsour.2021.229496.

Kriston, Akos; Adanouj, Ibtissam; Ruiz, Vanesa; Pfrang, Andreas (2019): Quantification and simulation of thermal decomposition reactions of Li-ion battery materials by simultaneous thermal analysis coupled with gas analysis. In: *Journal of Power Sources* 435, S. 226774. DOI: 10.1016/j.jpowsour.2019.226774.

Lenz, Carolin (2024): Analyse des Reaktionsverhaltens beim thermischen Durchgehen einer Batteriezelle. Universitätsbibliothek Braunschweig.

Lenz, Carolin; Hennig, Jakob; Tegethoff, Wilhelm; Schweiger, Hans-Georg; Koehler, Juergen (2023): Analysis of the Interaction and Variability of Thermal Decomposition Reactions of a Li-Ion Battery Cell. In: *J. Electrochem. Soc.* DOI: 10.1149/1945-7111/acd964.

MacNeil, D. D.; Dahn, J. R. (2001): Test of Reaction Kinetics Using Both Differential Scanning and Accelerating Rate Calorimetries As Applied to the Reaction of Li x CoO 2 in Non-aqueous Electrolyte. In: *J. Phys. Chem. A* 105 (18), S. 4430–4439. DOI: 10.1021/jp001187j.

OpenSCALING (2023). Online verfügbar unter https://openscaling.org/, zuletzt geprüft am 19.03.2025.

Ren, Dongsheng; Liu, Xiang; Feng, Xuning; Lu, Languang; Ouyang, Minggao; Li, Jianqiu; He, Xiangming (2018): Model-based thermal runaway prediction of lithium-ion batteries from kinetics analysis of cell components. In: *Applied Energy* 228, S. 633–644. DOI: 10.1016/j.apenergy.2018.06.126.

Schöberl, Jan; Ank, Manuel; Schreiber, Markus; Wassiliadis, Nikolaos; Lienkamp, Markus (2024): Thermal runaway propagation in automotive lithium-ion batteries with NMC-811 and LFP cathodes: Safety requirements and impact on system integration. In: *eTransportation* 19, S. 100305. DOI: 10.1016/j.etran.2023.100305.

TIL Suite. Version 2024.01: TLK-Thermo GmbH. Online verfügbar unter https://www.tlk-thermo.com/en/software/til-suite, zuletzt geprüft am 14.03.2025.

TILMedia Suite. Version 2024.01: TLK-Thermo GmbH. Online verfügbar unter https://www.tlk-thermo.com/en/software/tilmedia-suite, zuletzt geprüft am 14.03.2025.

Uddin, Kotub; Picarelli, Alessandro (2014): Phenomenological Li ion battery modelling in Dymola. In: Proceedings of the 10th International Modelica Conference, March 10-12, 2014, Lund, Sweden. the 10th International Modelica Conference, March 10-12, 2014, Lund, Sweden, March 10-12, 2014: Linköping University Electronic Press (Linköping Electronic Conference Proceedings), S. 327–334.

Walker, William Q.; Bayles, Gary A.; Johnson, Kenneth L.; Brown, Ryan P.; Petrushenko, David; Hughes, Peter J. et al. (2022): Evaluation of Large-Format Lithium-Ion Cell Thermal Runaway Response Triggered by Nail Penetration using Novel Fractional Thermal Runaway Calorimetry and Gas Collection Methodology. In: *J. Electrochem. Soc.* 169 (6), S. 60535. DOI: 10.1149/1945-7111/ac7897.

Wang, Yu; Ren, Dongsheng; Feng, Xuning; Wang, Li; Ouyang, Minggao (2022): Thermal runaway modeling of large format high-nickel/silicon-graphite lithium-ion batteries based on reaction sequence and kinetics. In: *Applied Energy* 306, S. 117943. DOI: 10.1016/j.apenergy.2021.117943.

Wendland, Robert; Padberg, Pascal; Tegethoff, Wilhelm; Koehler, Juergen (2018): Dynamic Optimization of Thermal Management and Cooling Plate Design for Battery Systems. 27th Aachen Colloquium Automobile and Engine Technology. Aachen.